

SMAI-JCM
SMAI JOURNAL OF
COMPUTATIONAL MATHEMATICS

Refinement for a Hybrid Boundary
Representation and its Hybrid
Volume Completion

YANG SONG & ELAINE COHEN

Volume S5 (2019), p. 3-25.

<http://smajcm.centre-mersenne.org/item?id=SMAI-JCM_2019__S5__3_0>

© Société de Mathématiques Appliquées et Industrielles, 2019

Certains droits réservés.



Publication membre du

Centre Mersenne pour l'édition scientifique ouverte

<http://www.centre-mersenne.org/>

Sousmission sur <https://smajcm.math.cnrs.fr/index.php/SMAI-JCM>



Refinement for a Hybrid Boundary Representation and its Hybrid Volume Completion

YANG SONG¹
ELAINE COHEN²

¹ School of Computing, University of Utah, Salt Lake City, UT, USA

E-mail address: yangsong@cs.utah.edu

² School of Computing, University of Utah, Salt Lake City, UT, USA

E-mail address: cohen@cs.utah.edu.

Abstract. With the increasing need for volumetric B-spline representations and the lack of methodologies for creating semi-structured volumetric B-spline representations from B-spline Boundary Representations (B-Rep), hybrid approaches combining semi-structured volumetric B-splines and unstructured Bézier tetrahedra have been introduced, including one that transforms a trimmed B-spline B-Rep first to an untrimmed Hybrid B-Rep (HB-Rep) and then to a Hybrid Volume Representation (HV-Rep). Generally, the effect of *h-refinement* has not been considered over B-spline hybrid representations. Standard refinement approaches to tensor product B-splines and subdivision of Bézier triangles and tetrahedra must be adapted to this representation. In this paper, we analyze possible types of *h-refinement* of the HV-Rep. The revised and trim basis functions for HB- and HV-rep depend on a partition of knot intervals. Therefore, a naive *h-refinement* can change basis functions in unexpected ways. This paper analyzes the effect of *h-refinement* in reducing error as well. Different *h-refinement* strategies are discussed. We demonstrate their differences and compare their respective consequential trade-offs. Recommendations are also made for different use cases.

2010 Mathematics Subject Classification. 65D17.

Keywords. *h-refinement*, Trimmed model, Volume completion.

1. Introduction

The most common representation in CAD is the Boundary Representation (B-rep), which typically uses parametric Non-Uniform B-Splines (NURBS) for each surface in the model. Trimming, a common technique in constructing complex geometries results when Boolean operations are applied to models. In those models, only restricted parts of the original surfaces visibly appear in the final models. With the recent development of Isogeometric Analysis (IGA), there is an increasing need for both watertight and volumetric representations of B-reps, including those with trimmed surfaces.

In general, trimmed models cannot be represented exactly as tensor product B-splines, and so are not watertight. In commercial CAD systems, trimming curves exist in the parametric domains of intersecting B-spline surfaces and in model (or Euclidean) space, usually approximated as linear or cubic B-spline curves. The three trimming curve representations do not lead to the exact same model space curves, so there are gaps or overlaps between trimmed surfaces. The Euclidean trimming curve is typically not in either surface. However, models for analysis must be watertight. Models to be realized with additive fabrication are typically triangulated. If the triangles generated from the two surfaces across a trimming curve are not *close enough* the model is not suitable for fabrication. Post design industries have grown around repairing inconsistent geometric models for both fabrication and analysis. Typically, for analysis, that has been done through mesh creating and mesh mending. If the original geometric model representation is a watertight representation, there are no gaps to mend and the post modeling repair process is eliminated.

Another difficulty is that, while multiple methods have been proposed to generate a representation for volumetric completion from an untrimmed NURBS B-rep, in general, there is no method that

works for all untrimmed models, not to mention addressing trimmed ones. One principle of IGA is to use the CAD model basis as the parametric basis for the simulation representation [6], so maintaining the CAD representation on the boundary as closely as possible supports that goal. If the B-rep is semi-structured B-splines/NURBS, higher order continuity improves the quality of the simulation.

Hybrid representations have been proposed in [17, 18] to address these problems. This paper investigates ways in which refinement can affect both the hybrid boundary representation and the hybrid volume completion representation in these schemes that preserve the original surface parameterization.

In Section 2, we present related work. In Section 3 and 4, we briefly go through the steps to generate such watertight B-rep and volumetric representation. In Section 5, we categorize errors that exist in the HB-rep. In Section 6, we analyze different approaches to refinement and examine their effects on representation and computation.

2. Related Work

In order to create watertight representations from the intrinsic inexactness associated with the trimmed model, surface representations are necessarily modified, and frequently reparameterized in regions around the trimming curves, then remodeled to approximate the original surface with regular patches.

One approach changes the representation to T-splines [14] and modifies the surface parameterization near the trim while approximating the trimming curve according to a precision determined by the number of knot insertion T-levels. To merge two surfaces across their trimming curve further modifications are made using their proposed *NU-NURBS*. Another approach uses subdivision surfaces [15, 16], although the parameterization is modified and the geometry is approximated in at least a region of adjacent patches near the trim. These methods take advantage of the topological flexibility of these respective techniques and generate a unified control mesh/surface representation of the output model. Both are applicable when usage of those representations are desirable. However, as surveyed in [12], the trimmed B-spline still is the predominant technology in modeling.

Research into volumetric model completion from general boundaries has focused significant effort on starting with triangle mesh boundaries and generating semi-structures trivariate B-spline representations, for examples see [1, 2, 8, 9, 10, 25]. Efforts to complete and optimize a volumetric representation from a B-spline boundary mainly focused on a bounding hexahedron [23], or more general regions already partitioned into hexahedra [22]. Because there is no general approach to semi-structured trivariate B-spline volume completion while preserving the B-spline B-rep boundary, several approaches have been proposed that involve using tetrahedra.

Some approaches to volume completion preserve the B-spline boundary representation, yielding trivariate B-splines from the boundary to some depth depending on a user-provided mid-structure, and then transition to Bézier tetrahedra in the complex central region of the interior. [11] fills the rest of the interior with linear tetrahedral elements, although it allows gaps and overlaps between the trivariate B-splines and the linear tets. However, spline properties and the construction technique used ensure that as the B-splines are refined, the tetrahedra boundaries converge to the interior boundary of the trivariate B-spline. In [24], the interior is filled with high degree Bézier tetrahedra that reproduce the interior bounding surface of the trivariate B-spline. These hybrid approaches exploit the advantage of high accuracy of B-spline elements near the boundary. They also take advantage of the topological flexibility of the tetrahedra to complete the representations. However, the effects of h -refinement on the representation were not investigated.

[7] also describes an interior unstructured region filled with Bézier tetrahedra. They report on several different representations. All have unstructured tetrahedral regions. First, the tensor product Bézier patches are extracted from the boundary B-spline surfaces. Then one approach transforms each rectangular patch into 2 triangular Bézier patches along one diagonal, after which the interior

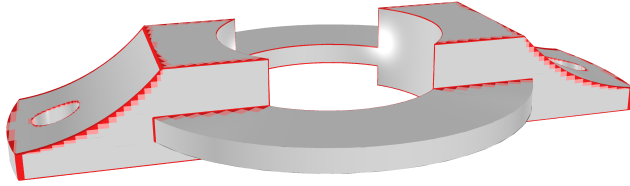


FIGURE 3.1. A mechanical part generated with multiple Boolean operations is shown in its HB-rep. Ω^{banded} , consisting of the red regions, is the transition region that approximates the surface while reproducing the trimming curves. It contains both tensor product and curvilinear triangle representations that touch the trimming curve. Because they represent the trimming curve exactly, even though the surface approximation is highly accurate, Ω^{banded} differs from the original surfaces in both parameterization and geometry.

is tetrahedralized. A different approach uses each Bézier patch as the base of a Bézier pyramid, then fills the remaining volume with tetrahedra. The last method creates a trivariate tensor product Bézier patch over each bivariate patch, and then uses either of the other two methods on its interior surface patches. [7] includes h -refinement schemes for the multiple element types.

[19] deals with completing trimmed B-spline representations into Bézier tetrahedra. It first decomposes the surfaces into Bézier patches. The work assumes that the three trimming curves representing the same intersection are not compatible; that is, they have independent knot vectors and independent parameterizations. The first effort makes them compatible by modifying parameterizations and knot vectors to ensure that the images of each knot value in model space all represent the same point. Then, after making the curves compatible, it refines all curves until they all can be approximated by piecewise linear curves within a user-specified accuracy in parametric space. A trimmed knot interval is a parametric knot interval that at least one trimming curve intersects. The *interior* of the trimmed knot interval is partitioned into multiple triangles. The surfaces are represented as degree 6 Bézier triangles, exactly representing the piecewise linear parametric trimming curves and the original surface in model space. Then coefficients of the Bézier triangles from different surfaces are modified along trimming curves to make them match and seal the representation.

The hybrid boundary and volumetric representation proposed for trimmed NURBS B-reps in [18] and [17], which is analyzed here, uses the ideas in [24] of both forming a trivariate spline and having an unstructured interior region that meets the structured region with C^0 continuity. However, this approach [17, 18] deals with the lack of a watertight boundary, and trimming curves, that cut parametric knot intervals into irregular pieces. The result largely keeps both the original parameterization and geometry except around the trimming curve where the geometry is modified to seal the representation. It does so by introducing *revised basis functions* wherever the supports of the B-spline basis functions overlap a trimming curve. It further introduces basis functions along the trimming curves whose support extends into a region around the trimming curve called Ω^{banded} . For model completion, the approach in [24] is generalized so the approach is suitable for a trimmed model. In this paper, we investigate and analyze h -refinement on the resulting HB-rep and HV-rep models.

3. HB-rep \mathcal{B}

In this section, we review the Hybrid Boundary Representation (HB-rep). A mechanical model representation produced from a trimmed NURBS B-rep is shown in Figure 3.1.

Let \mathcal{G} be the representation for a trimmed B-spline B-rep model, and let \mathcal{R} designate the collection of all control mesh points and control mesh adjacencies for all trimmed surfaces in \mathcal{G} . The HB-rep is

defined using refinement (and subdivision) properties of NURBS and B-splines. Let a B-spline surface in \mathcal{G} , say s , be defined in its untrimmed state as a degree bi- d B-spline surface,

$$s(\xi, \eta) = \sum_{i,j} r_{i,j} B_{i,d,\mu}(\xi) B_{j,d,\nu}(\eta),$$

where μ and ν are knot vectors. For $\mu_i, \mu_{i+1} \in \mu$ and $\nu_j, \nu_{j+1} \in \nu$, the rectangular parametric region $[\mu_i, \mu_{i+1}] \times [\nu_j, \nu_{j+1}]$ is called a *knot interval*, whenever it is non-degenerate. Given values $\xi_a < \xi_b$ and $\eta_c < \eta_d$ where there are no knot lines interior to the region $(\xi_a, \xi_b) \times (\eta_c, \eta_d)$, then s can be written in terms of tensor products of Bézier functions $\{\theta_{k_1,d, [\xi_a, \xi_b]}(\xi)\}_{k_1=0}^d$ and $\{\theta_{k_2,d, [\eta_c, \eta_d]}(\eta)\}_{k_2=0}^d$. This transformation to Bézier is easily accomplished by augmenting μ with multiple values of ξ_a, ξ_b to form $\tilde{\mu}$, and augmenting ν with multiples values of η_c, η_d , to form $\tilde{\nu}$ and computing coefficients $\alpha_{i,k_1,\mu,\tilde{\mu}}$ and $\alpha_{j,k_2,\nu,\tilde{\nu}}$ such that for $J^{\text{rect}} = [\xi_a, \xi_b] \times [\eta_c, \eta_d]$. We call J^{rect} a *sub-knot interval* when it is not a full knot interval of s ,

$$B_{i,d,\mu}(\xi) = \sum_{k_1} \alpha_{i,k_1,\xi} \theta_{k_1,d, [\xi_a, \xi_b]}(\xi) \quad \text{for } \xi \in [\xi_a, \xi_b], \quad (3.1)$$

$$B_{j,d,\nu}(\eta) = \sum_{k_2} \alpha_{j,k_2,\eta} \theta_{k_2,d, [\eta_c, \eta_d]}(\eta) \quad \text{for } \eta \in [\eta_c, \eta_d] \quad (3.2)$$

$$s(\xi, \eta) = \sum_{k_1, k_2} \left(\sum_{i,j} \alpha_{i,k_1,\xi} r_{i,j} \alpha_{j,k_2,\eta} \right) \theta_{k_1,d, [\xi_a, \xi_b]}(\xi) \theta_{k_2,d, [\eta_c, \eta_d]}(\eta) \quad \text{for } (\xi, \eta) \in J^{\text{rect}} \quad (3.3)$$

See [5]. Using Bézier extraction notation [3], and letting $N_{i,j}(\xi, \eta) = B_{i,d,\mu}(\xi) B_{j,d,\nu}(\eta)$, Equation 3.3 becomes

$$s(\xi, \eta) = \mathbf{r}^\top \mathbf{N}(\xi, \eta) = \mathbf{r}^\top \mathbf{A} \boldsymbol{\theta}_{J^{\text{rect}}}(\xi, \eta), \quad \forall (\xi, \eta) \in J^{\text{rect}}, \quad (3.4)$$

where \mathbf{r} is the vectorization of the coefficient matrix used to define the surface over J^{rect} , $\mathbf{N}(\xi, \eta)$ and $\boldsymbol{\theta}_{J^{\text{rect}}}(\xi, \eta)$ are the corresponding vectors, respectively, of tensor product B-spline and tensor product Bézier basis functions in J^{rect} , and $\mathbf{A} = \mathbf{A}_\xi \otimes \mathbf{A}_\eta$ the Kronecker tensor product of Bézier extraction operators in ξ and η directions for J^{rect} of size $(d+1)^2 \times (d+1)^2$ [3]. Thus each B-spline can be evaluated over the whole surface or any rectangular patch in terms of related Bézier functions. This property is used repeatedly.

For each surface in \mathcal{G} , the methodology for the HB-rep consists of,

- (1) For each trimmed knot interval K , construct a rectilinear approximation to the trimming curve that does not touch it and is completely interior to the trimmed surface. The region Ω^{banded} is bounded by the rectilinear approximation and the trimming curve illustrated by the orange polyline in Fig. 3.2d, and is created using the *subknot intervals* that touch trimming curves, as shown. Changes from the original surface to seal the representation can occur only inside Ω^{banded} .
- (2) Create basis functions for the new representation.
 - The *revised basis functions* are identical to B-splines outside Ω^{banded} and continuously decrease to evaluate to 0 on the trimming curve inside Ω^{banded} .
 - Define *trim functions* with support in Ω^{banded} that form a partition of unity on the trimming curve and are linearly independent.
- (3) Determine coefficients for the new trim basis functions, merging the pieces of the trim basis functions over multiple intervals in Ω^{banded} , to complete the watertight representation and match the model space trimming curve. In Figure 3.1, the image of Ω^{banded} in model space is colored red. The representation is called a Hybrid Boundary Representation (HB-rep).

- (4) The region in each trimmed knot interval minus Ω^{banded} , $K - \Omega^{\text{banded}}$, is a rectilinear region, see Fig. 3.2d It is represented by the original surface. However, when the hybrid volume representation is created [17], the innermost unstructured tetrahedral region uses sub-knot intervals from which to derive the tetrahedralization on the interface between the regions. Hence, we also support partitioning $K - \Omega^{\text{banded}}$ into interior sub-knot intervals with locally optimal shape properties. See Fig. 3.2e and Fig. 3.3. Call the partition \mathcal{K} .

The resulting HB-rep consists of the coefficients and revised basis functions, the trim basis functions and their coefficients, and the partitionings derived in step 4. Also, the information defining the original trimmed B-rep is embedded.

Steps 1 and 4 are illustrated in Figure 3.2. Recall the term *knot interval* is used herein to denote a tensor product of the intervals between knots, one interval in each parametric direction of an original surface. A knot interval in \mathcal{G} is classified into 3 groups as *interior*, *trimmed*, and *exterior*, based on its relative position with respect to the trimming curves. Each *trimmed knot interval* is crossed by or touches a trimming curve along a boundary, so it has regions that are interior and either exterior or on the trimming curve. Each trimmed knot interval is further partitioned into a set of *sub-knot intervals*. The sub-knot intervals are divided into 2 collections: those that are interior defining \mathcal{K} , and those that define a region called Ω^{banded} that is adjacent to the trimming curves. New functions, called *revised basis functions*, are defined, one for each B-spline in the original representation. Each new function is defined to be identical to its corresponding original B-spline except in Ω^{banded} . Hence, over interior knot intervals and interior sub-knot intervals, the new representation remains unchanged. Additional functions called *trim basis functions* are defined in Ω^{banded} that carry trimming curve and Ω^{banded} geometry and parametric information, and serve to seal the gaps and retract the overlaps.

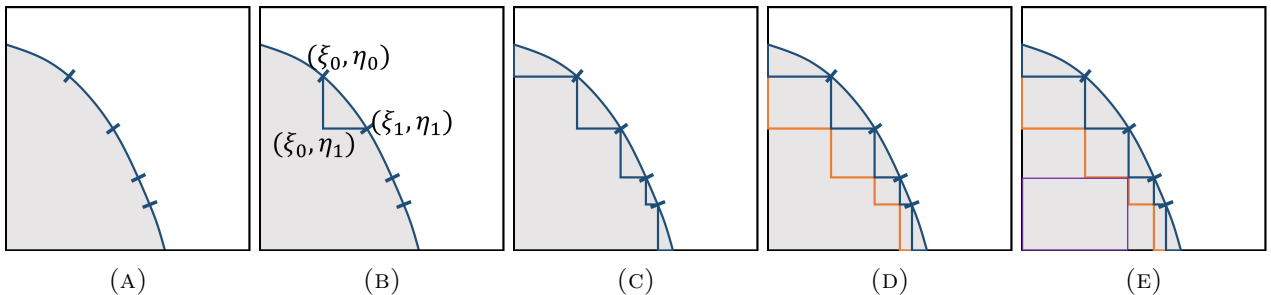


FIGURE 3.2. Parametric domain process to generate Ω^{banded} and a partition is shown of a trimmed knot interval. The retained portion of the interval is in gray. (a) shows a trimming curve with 5 Bézier segments passing through the trimmed knot interval. (b) shows the rectilinear approximation and curvilinear triangle for one trimming Bézier segment. Similarly, this is repeated for each Bézier trimming curve segment with results shown in (c). In (d) rectangular sub-knot intervals are created that have one corner point on the trimming curve. Ω^{banded} is the region between the orange rectilinear curve and the trimming curve. Finally, in (e), the remainder of the parametric trimmed knot interval is recursively partitioned into internal rectangular sub-knot intervals. In this particular example, the large purple rectangle is chosen first, having the best ratio of the lengths of the sides. This leaves two rectangles to form the other elements of the partition.

Define Ω^{banded} . Given a trimming curve across two surfaces, each of the two parametric trimming curves and the model space trimming curve need to be compatible. That is, they need to have the

same knot values and parameterizations, and the model space values of the same knot values need to represent the same points on the model space curves. If the output of the CAD system does not produce this, then the method in Xia [19] is adopted to produce this result. Knots are added to the trimming curves each time either of the parametric curves crosses a knot line in either parametric domain. Then the curves are subdivided to Bézier segments. Each Bézier segment is further subdivided at interior local extremal points of either parametric curve so each final Bézier curve segment is monotonic.

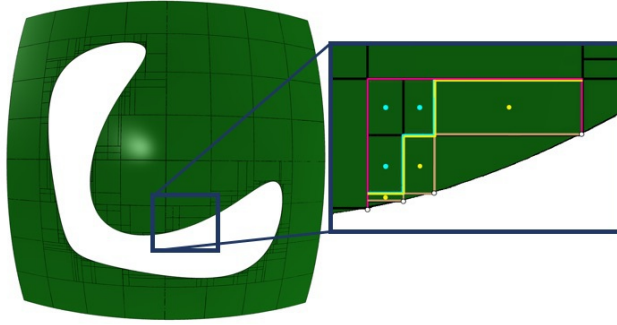


FIGURE 3.3. A valid partitioning example. The inset shows a trimmed knot interval (bounded by magenta isoparametric lines). It is further decomposed into regions by the yellow and cyan line, namely, (i) Ω^{banded} consists of curvilinear triangular and rectangular sub-knot intervals that are adjacent to the trimming curve; and region (ii), the rectilinear region (cyan dots in interior sub-knot intervals).

At this stage, the trimming curve defining a trimmed knot interval may have multiple segments. (See Figure 3.2a.) A rectilinear approximation is built for each segment. Given a Bézier segment with endpoints at (ξ_0, η_0) , and (ξ_1, η_1) , assume without loss of generality that (ξ_0, η_1) is in the interior of the trimmed domain. The rectilinear approximation to the Bézier segment is found by connecting the two endpoints to (ξ_0, η_1) , see Figure 3.2b. The region between the Bézier segment and its rectilinear approximation defines a curvilinear triangular sub-knot interval. In Figure 3.2c, the rectilinear approximations, and their corresponding curvilinear triangular sub-knot intervals to all the Bézier segments in the trimmed knot interval are indicated. Every trimming curve endpoint that is not a local extremum corresponds to a rectangular sub-knot interval that has a corner at the endpoint and shares edges with its two adjacent curvilinear triangular sub-knot intervals. In Figure 3.2d, these are the rectangles with orange and blue sides. The shared edges must have exactly the same two endpoints on its two sides, or an inconsistency occurs [17].

If instead, a Bézier segment is isoparametric with endpoints (ξ_0, η_0) and (ξ_0, η_1) , a suitable rectilinear approximation is found, with corners (ξ_0, η_0) , (ξ_1, η_0) , (ξ_1, η_1) , (ξ_0, η_1) where ξ_1 is obtained by extending ξ_0 into the interior for a predetermined minimum feature size. In this case, the region between the Bézier curve and its rectilinear approximation is a rectangular sub-knot interval.

At this stage, each sub-knot interval generated should have at least one corner on the trimming curve. The set of all sub-knot intervals is denoted Ω^{banded} . Examples of Ω^{banded} are illustrated in Figure 3.2d in the parametric domain and in Figure 3.3 in model space.

Revised and Trim Basis Functions. Each original B-spline basis function $N_{i,j}$ that has support in Ω^{banded} is modified into a revised basis function $\tilde{N}_{i,j}$ over its support in Ω^{banded} such that it continuously decreases and is 0 along any of its trimming curve intersections. (See Figure 3.4a.) Trim basis functions are introduced to compensate for the modification and glue together surfaces across the trimming curve. Also, in [17, 18] it is shown that the important partition of unity property obtains for the combined set of new basis functions.

As a result of the preceding process, a sub-knot interval in Ω^{banded} is either an isoparametric rectangular sub-knot interval, denoted J^{rect} , or a curvilinear triangular sub-knot interval, denoted J^{tri} . The sub-knot interval has been trimmed by the trimming curve according to one of the following three configurations: (i) at least one isoparametric edge of J^{rect} resides on a trimming curve, (ii) a corner of J^{rect} is on the trimming curve, or (iii) the curvilinear edge of J^{tri} is part of trimming curve.

For J^{rect} , the tensor product Bézier functions defining its surface mapping are partitioned into two sets: those that vanish on the trimming curve and those that are nonzero. Let the identity matrix be $I = (e_{i,j})$ where $e_{i,j} = \delta_{i,j}$, the Kronecker δ . A *masking* matrix M^{rect} is formed by modifying the identity matrix I so that if the k -th basis function in $\boldsymbol{\theta}^{\text{rect}}$ is nonzero on the trimming curve, then $e_{k,k} = 0$. This results in M^{rect} having a zero vector for column k . M^{rect} differs for each J^{rect} . The surface is

$$\begin{aligned} s(\xi, \eta) &= \mathbf{r}^\top \mathbf{N}(\xi, \eta) = \mathbf{r}^\top \mathbf{A} M^{\text{rect}} \boldsymbol{\theta}_{J^{\text{rect}}}(\xi, \eta) + \mathbf{r}^\top \mathbf{A} (I - M^{\text{rect}}) \boldsymbol{\theta}_{J^{\text{rect}}}(\xi, \eta) \\ &= \mathbf{r}^\top \tilde{\mathbf{N}}|_{J^{\text{rect}}}(\xi, \eta) + \mathbf{r}^\top \mathbf{A} \tilde{\mathbf{T}}|_{J^{\text{rect}}}(\xi, \eta), \forall (\xi, \eta) \in J^{\text{rect}}, \end{aligned}$$

where $\tilde{\mathbf{N}}|_{J^{\text{rect}}} = \mathbf{A} M^{\text{rect}} \boldsymbol{\theta}_{J^{\text{rect}}}$ and $\tilde{\mathbf{T}}|_{J^{\text{rect}}} = (I - M^{\text{rect}}) \boldsymbol{\theta}_{J^{\text{rect}}}$ are the vectors of *revised* and *trim* basis functions, respectively, in J^{rect} . To reproduce the trimmed surface, the coefficients for $\tilde{\mathbf{T}}$ are $\mathbf{r}^\top \mathbf{A}$. However, when the representation is coerced to become watertight, the coefficients for $\tilde{\mathbf{T}}$ are modified to be coefficient(s) of its defining Bézier trimming curve segment.

Without loss of generality, suppose the curvilinear triangle has 3 corners at (ξ_0, η_0) , (ξ_1, η_0) , and (ξ_0, η_1) with 2 isoparametric edges and 1 Bézier trimming curve edge, as in Figure 3.2b. The geometry is approximated with a degree d polynomial that matches the trimming curve exactly. Let Δ be the triangle with the same corners as J^{tri} . Define $\phi : \Delta \rightarrow J^{\text{tri}}$ to be a degree d triangular Bézier mapping that is the identity on the isoparametric edges and reproduces the degree d parametric Bézier trimming curve boundary exactly and has no folds or degeneracies. For simplicity of presentation, suppose that $d = 3$, and let ψ be a cubic Bézier triangle mapping from triangle Δ to model space with geometry approximating s and that matches s on the two isoparametric boundaries of J^{tri} . Coefficient computations for both ϕ and ψ are detailed in [17, 18] that make the coefficients of ψ dependent on \mathbf{r} . With the help of a *selection* matrix S^{tri} and Bézier extraction operator \mathbf{A} in $(\xi_0, \xi_1) \times (\eta_0, \eta_1)$, ψ 's coefficient row vector is written in form of $\mathbf{r}^\top \mathbf{A} S^{\text{tri}}$. The mapping $\psi \circ \phi^{-1}(\xi, \eta)$ is then used to approximate the original B-spline surface mapping from J^{tri} . The control points for the non-isoparametric edge, including the corner vertices will be modified to be control points of a trimming segment.

Again, using Bézier extraction notation, where $\boldsymbol{\theta}_{J^{\text{tri}}}$ is the vector of triangular Bézier basis functions over J^{tri} , the *curvilinear triangle basis functions* used to define $\psi \circ \phi^{-1}$ are $\boldsymbol{\theta}_{J^{\text{tri}}} \circ \phi^{-1}$. While the $\psi \circ \phi^{-1}$ is C^0 across adjacent sub-knot interval boundaries, it is no longer polynomial. Analogous to the rectangular case, a $\frac{1}{2}(d+1)(d+2) \times \frac{1}{2}(d+1)(d+2)$ masking matrix M^{tri} is used to segregate the functions in $\boldsymbol{\theta}_{J^{\text{tri}}} \circ \phi^{-1}$ into those that vanish along the trimming curve and those that are nonzero. Specifically, $\boldsymbol{\theta}_{J^{\text{tri}}} \circ \phi^{-1}$ is used to *replace* the tensor product Bézier basis functions $\boldsymbol{\theta}_{J^{\text{rect}}}$, and so realize a curvilinear (non-polynomial) triangular approximation of the original B-spline surface in J^{tri} . Thus,

$$\begin{aligned} \mathbf{r}^\top \mathbf{N}(\xi, \eta) &\approx \psi \circ \phi^{-1}(\xi, \eta) = \mathbf{r}^\top \mathbf{A} S^{\text{tri}} (I - M^{\text{tri}}) \boldsymbol{\theta}_{J^{\text{tri}}} \circ \phi^{-1}(\xi, \eta) \\ &= \mathbf{r}^\top \tilde{\mathbf{N}}|_{J^{\text{tri}}}(\xi, \eta) + \mathbf{r}^\top \mathbf{A} S^{\text{tri}} \tilde{\mathbf{T}}|_{J^{\text{tri}}} \circ \phi^{-1}(\xi, \eta), \forall (\xi, \eta) \in J^{\text{tri}}, \end{aligned}$$

where $\tilde{\mathbf{N}}|_{J^{\text{tri}}} = \mathbf{A} S^{\text{tri}} M^{\text{tri}} \boldsymbol{\theta}_{J^{\text{tri}}} \circ \phi^{-1}$ and $\tilde{\mathbf{T}}|_{J^{\text{tri}}} = (I - M^{\text{tri}}) \boldsymbol{\theta}_{J^{\text{tri}}} \circ \phi^{-1}$ are the revised and trim basis functions, respectively, in J^{tri} .

Figure 3.4 illustrates a simple example. Figure 3.4a shows a particular trimmed B-spline and its revised counterpart. Although both have trimmed domains, the B-spline is nonzero along its trimming curve, but the revised function has continuously diminished to 0 over Ω^{banded} . Figure 3.4b shows the partition of a trimmed knot interval $[0, 1] \times [0, 1]$. Originally, 16 B-spline basis functions $N_{i,j}$ for

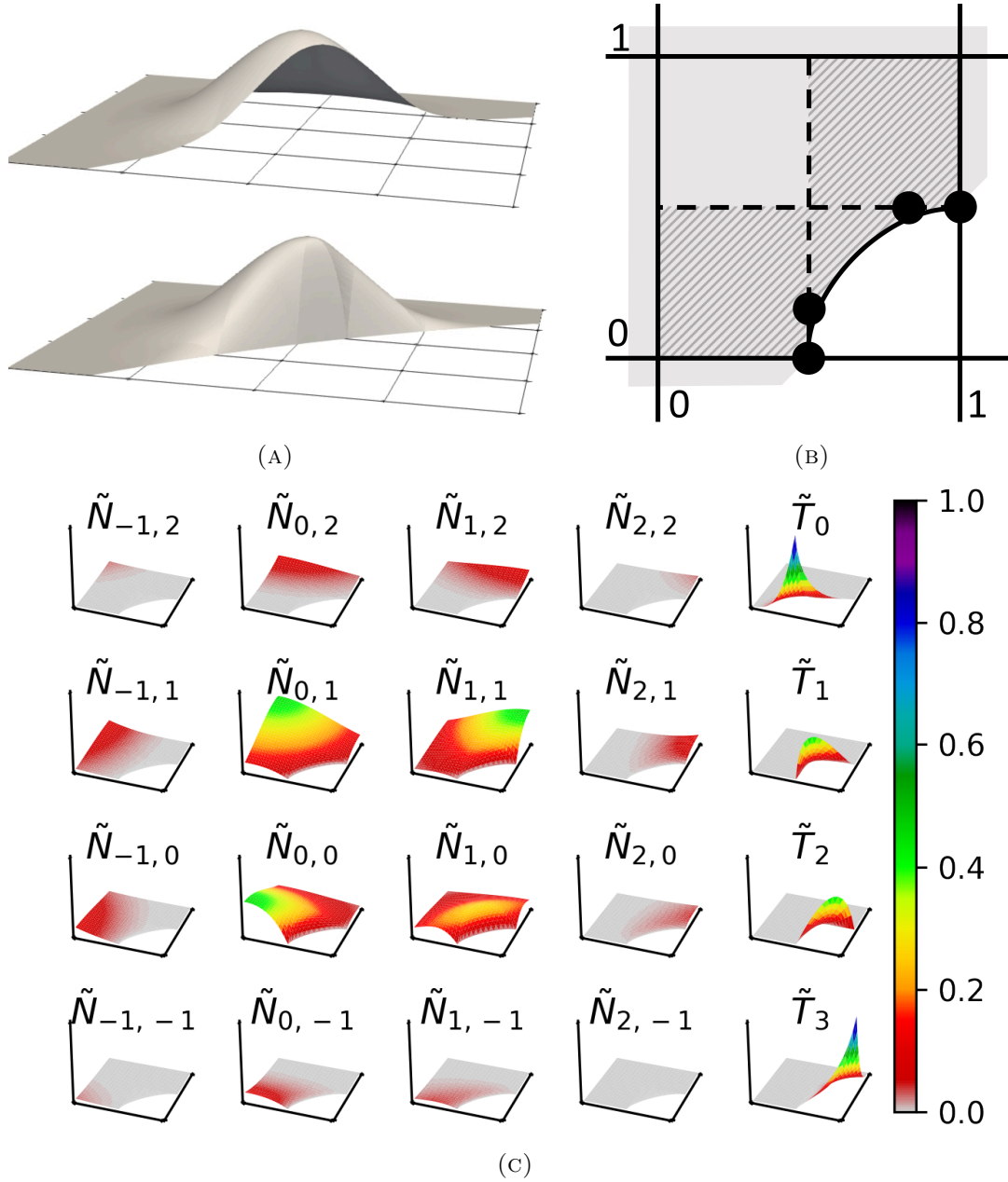


FIGURE 3.4. A trimmed B-spline basis function (a) top $N_{0,0}$ and its revised counterpart (a) bottom. $\tilde{N}_{0,0}$. In (b), the partition of knot interval $[0, 1] \times [-1, 0]$ consists of 4 sub-knot intervals: 3 rectangular and 1 curvilinear triangular. Ω^{banded} is represented by the hatched region, and the 4 black dots represent the control points of the trimming curve. (c) shows all of the 16 revised B-spline basis functions $\tilde{N}_{i,j}$ and 4 trim basis functions \tilde{T}_i corresponding to the 4 dots.

$i \in \{-1, 0, 1, 2\}, j \in \{-1, 0, 1, 2\}$ existed over this domain corresponding to their 16 original control points. Two types of new basis functions now exist: (i) 16 revised B-spline basis functions $\tilde{N}_{i,j}$ that are different from original ones only in Ω^{banded} , and forced to be identically 0 on the trimming curve; (ii) 4 trim basis functions \tilde{T}_i for $i \in \{0, 1, 2, 3\}$ with coefficients that correspond to 4 control points

of the Euclidean cubic trimming curve (Figure 3.4c). Outside of Ω^{banded} , all $\tilde{T}_i \equiv 0$, and $\tilde{N}_{i,j} \equiv N_{i,j}$. The extraction relationship between the original surface and the sub-knot interval is maintained.

Seal the Trim. During the construction of the new basis functions, each trim basis function is initially associated with a control point from $\mathbf{r}^\top \mathbf{A}$. The control points corresponding to basis functions that are nonzero on the trimming curve are replaced with control points from the model space trimming curve c_m . The set of all control points that are coefficients of trim basis functions is denoted Υ . By combining trim basis functions corresponding to the same control point in different sub-knot intervals across trimming curves, C^0 basis functions are constructed, and the new representation \mathcal{B} is watertight, as illustrated in Figure 3.5. With \mathcal{R} correspond to revised basis functions and Υ correspond to trim basis, no extra degrees of freedom are added to \mathcal{B} . The total degrees of freedom is $|\mathcal{R}| + |\Upsilon|$.

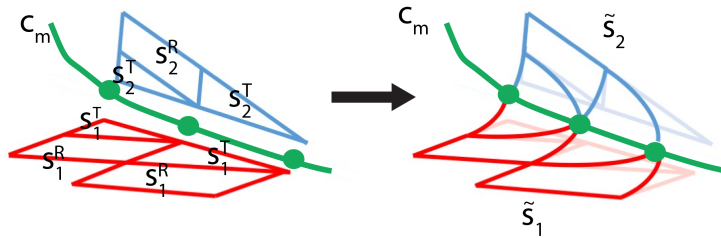


FIGURE 3.5. Making the representation watertight. Two trimmed surfaces that intersect at c_m (green) in model space. Representations of each surface over its J^{rect} and J^{tri} in Ω^{banded} are shown to not actually coincide. Then the appropriate coefficients of the trim basis functions are modified so that the model space trimming curve bounds on both the red and blue surfaces.

The remainder partition. After Ω^{banded} is created in a trimmed knot interval, the residual part of the trimmed knot interval is a rectilinear region. All evaluations and properties can be computed over this region using the B-splines that define the original surface, but if that choice is made, it would have to be verified for each evaluation that the point is not in Ω^{banded} . Instead, the residual is partitioned into interior rectangular sub-knot intervals whose local surface representations are defined as in Equations 3.1, 3.2, and 3.3. One construction goal is to make the resulting sub-knot intervals as square as possible. However, according to [13], finding an optimal solution to this problem is considered NP-hard. Therefore, a greedy divide-and-conquer approach was introduced in [17, 18] to resolve the problem recursively (see Figures 3.2e and 3.3). Let \mathcal{K} be the resulting collection of interior axis aligned sub-knot intervals. Note that B-splines with support in any element of \mathcal{K} can be written in terms of the corresponding Bézier functions over that rectangular region.

Example. In Figure 3.1, a mechanical part with multiple trimming curves has been converted to an HB-rep. The size of the curvilinear triangles on the flat surfaces is constrained only by the trimming curves since the geometry can be represented exactly. In this image, Ω^{banded} has been reduced in order to maintain the original representation everywhere except in the red regions. In those regions, the new representation, a perturbation of the original, is exact, up to trimming curve error.

4. HV-rep \mathcal{V}

In previously related work [11, 24] completed untrimmed B-spline B-rep models to form hybrid volumes. The approach forms trivariate splines by extending meshes inward from the exterior towards a mid-structure to some depth. The remaining interior is then filled with unstructured compatible Bézier tetrahedra. In [17] the volume completion problem is addressed in the more general and more challenging context of trimmed B-spline B-rep models. In particular, control meshes of trimmed B-splines do not form manifolds, an attribute that was critical to previous hybrid approaches to volume completion on untrimmed models.

The methodology in creating the Hybrid Volume Representation (HV-rep) goes according to the following steps:

- (1) Input an HB-rep \mathcal{B} and a mid-structure \mathcal{M} , as well as several parameters, where one of them is the number of control levels in the final trivariate spline, say n . Note that the information in \mathcal{G} is contained in \mathcal{B} .
- (2) Create a vector field for tracing the control points in \mathcal{R} from the given boundary surface to the mid-structure \mathcal{M} . Set $\mathcal{R}^0 = \mathcal{R}$.
- (3) Proceed through the following process, for i from 1 to n ,
 - (a) Trace each control point in \mathcal{R}^{i-1} from its current location to the mid-structure and compute its length.
 - (b) Normalize the newly computed length to $\frac{n-i+1}{n}$, and move along the trace a scaled distance of $\frac{1}{n}$. These new points form the initial i^{th} control mesh layer $\mathcal{R}_{\text{tr}}^i$. Since it is likely that when the trimming curves are applied, the surfaces do not match along their trims, they must be adjusted.
 - (c) Apply a least squares process to adjust the surfaces so the trimmed surfaces edges are close to each other, forming $\mathcal{R}_{\text{lstsq}}^i$.
 - (d) Move the surfaces apart so that there is a small separation gap around each trimming curve (i.e., the surfaces do not overlap), forming $\mathcal{R}_{\text{sep}}^i$.
 - (e) Form \mathcal{R}^i by applying mesh smoothing (as in [11, 24]) so the spacing of the tracings is more uniform.
 - (f) Using Ω^{banded} , the revised and trim basis functions, seal the layer and create \mathcal{B}^i .

In a 2-D scenario, Figure 4.1 illustrates some of the issues while describing our solution approach.

The input is the HB-rep \mathcal{B} , a mid-structure \mathcal{M} , and parameters, including n , the number of inward trajectory layers, along with depth factor ω , scalar for separating ϵ , relaxation factor β and θ that defines pyramid layer thickness. In the naming convention, the superscript designates the corresponding layer, and the subscript refers to the stage in each layer such as $\mathcal{R}_{\text{tr}}^i$ and \mathcal{G}^i , for example.

4.1. Trace \mathcal{R}

In order to create a suitable field that can serve to guide us in constructing the control point trace paths, it is first necessary to create an appropriate polyhedron. To do so, a triangle mesh is created from each trimmed surface by dividing each control mesh quadrilateral into two triangles. Then the Boolean operations used to create \mathcal{G} are applied to the corresponding triangle meshes to generate a polyhedron \mathcal{P} . The control meshes input as part of \mathcal{B} should have been previously refined sufficiently so \mathcal{P} has the same topology as \mathcal{B} . In Figure 4.1a the intersected control polygon for the curves serves as the polygon. Then the points of \mathcal{R} are separated into 2 disjoint covering subsets: \mathcal{E} contains those control points that are on \mathcal{P} and $\mathcal{R} - \mathcal{E}$ contains those that are not. In Figure 4.1, $P_{i+2}, P_{i+3}, Q_j, Q_{j+1} \in (\mathcal{R} - \mathcal{E})$.

HYBRID REFINEMENT

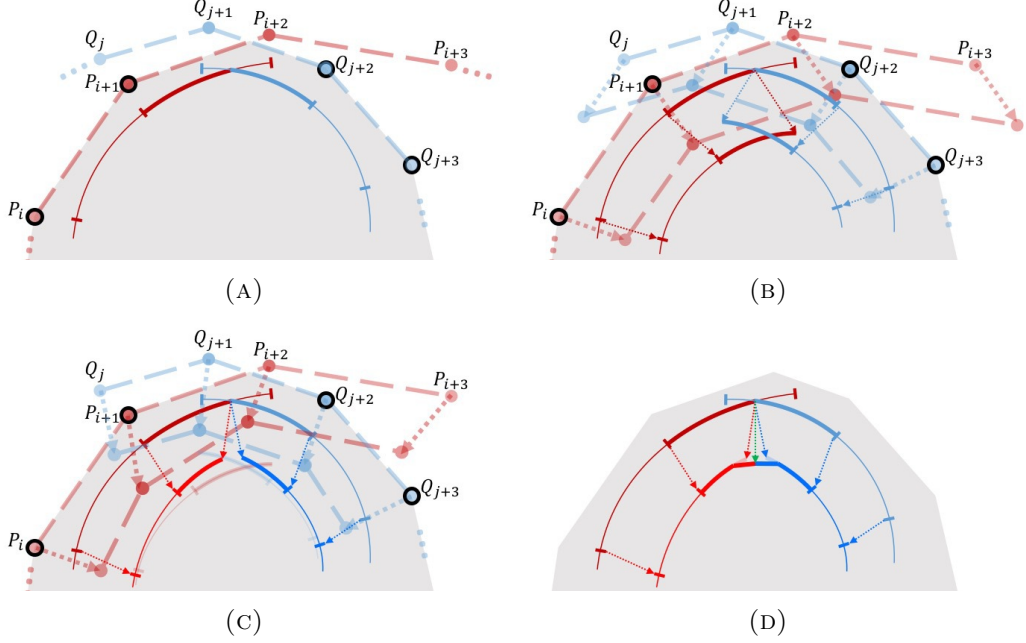


FIGURE 4.1. A 2D example of our approach. (a) An intersection of two curves with associated control polygons ($P_i \dots P_{i+3}$ and $Q_i \dots Q_{i+3}$) uses only part of the curves (thick strokes). Control points are separated into two groups: \mathcal{E} (colored dots in black circles) and $\mathcal{R} - \mathcal{E}$. In (b) paths for control points in \mathcal{E} are traced appropriately being guided by a harmonic gradient vector field while inward trajectories for $\mathcal{R} - \mathcal{E}$ are generated using the trajectories from their mesh neighbors (Section 4.1). Resulting curves might intersect with each other, so this is resolved in Section 4.2 (c). In (d), endpoints of traced trimmed curve are adjusted to their midpoint, thus sealing the gap.

Further, let $\mathcal{O}_{\mathcal{E}} = \{r \in \mathcal{E} : \text{there is an edge in } \mathcal{R} \text{ joining } r \text{ to a point in } \mathcal{R} - \mathcal{E}\}$ and define $\mathcal{O}_{\mathcal{R}-\mathcal{E}}$ analogously. Define $\mathcal{O} = \mathcal{O}_{\mathcal{E}} \cup \mathcal{O}_{\mathcal{R}-\mathcal{E}}$. In Figure 4.1, $P_{i+1}, Q_{j+2} \in \mathcal{O}_{\mathcal{E}}$. Geometrically, the control points in \mathcal{O} are close to the trimming curves.

The control points of \mathcal{E} are traced inward towards \mathcal{M} by following a vector field. A discrete harmonic function h is created with increasing values from boundary \mathcal{P} to mid-structure \mathcal{M} . The vector field \mathbf{f} used is a blend of the gradient of the harmonic function h and the gradient of a signed distance function g : $\mathbf{f} = h \frac{\nabla h}{\|\nabla h\|} + (1 - h) \nabla g$.

For each vertex in \mathcal{E}^i , the tracing curve to find $\mathcal{E}_{\text{tr}}^{i+1}$ terminates at harmonic value 1 (on \mathcal{M}). Normalized arc length parameterizations of the tracing curve are reparameterized to the parametric domain $[\frac{i}{n}\omega, 1]$; and the point at parametric value $\frac{i+1}{n}\omega$ is assigned to $\mathcal{E}_{\text{tr}}^{i+1}$. As control points in $\mathcal{R} - \mathcal{E}$ are not on \mathcal{P} , they cannot be traced. Instead, for $p \in \mathcal{R} - \mathcal{E}$, a breadth-first search is applied to the control mesh to find the $q \in \mathcal{E}$ closest to p in Euclidean distance. A translated copy of the tracing of q is used.

Control mesh $\mathcal{R}_{\text{tr}}^i$, along with the original basis functions of \mathcal{G} and parametric trimming curves result in an initial trimmed surfaces layer $\mathcal{G}_{\text{tr}}^i$.

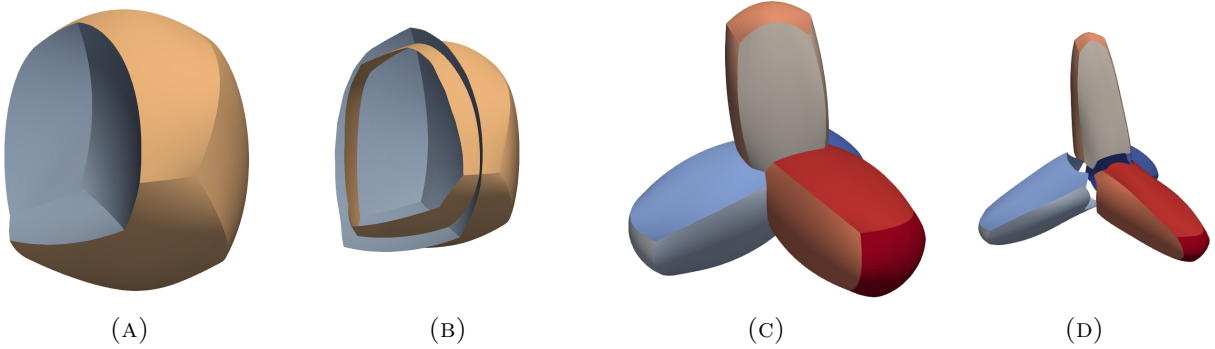


FIGURE 4.2. HB-rep models are shown in (a) and (c). When only tracing is applied, self-intersections are typically found in models that involve either Boolean intersection or subtractions (b). Tracing on model that only has union operations leads to gaps around trimming curves (d).

4.2. Adjust $\mathcal{R}_{\text{tr}}^i$

By following the tracing, the resulting $\mathcal{G}_{\text{tr}}^i$ is not a manifold as illustrated in Figures 4.2b and 4.2d. $\mathcal{R}_{\text{tr}}^i$ are adjusted so that the resulting trimmed surfaces do not intersect and corresponding trimming curve pairs on different surface pieces are close to each other. This section discusses Step 3c through Step 3e in Section 4.

The least squares fit adjusts the control points in \mathcal{O}^i . Along a trimming curve, associated curves c_1, c_2 exist in the parametric domains of two trimmed surfaces $s_{1,\text{tr}}^i, s_{2,\text{tr}}^i$, respectively. We start by sampling over the trimming curve with parameter t . For each sample t on the parametric trimming curves, the reference position of the Euclidean trimming curve is computed from both sides as their midpoint, $c_{e,\text{tr}}^i(t) = \frac{1}{2}(s_{1,\text{tr}}^i c_1(t) + s_{2,\text{tr}}^i c_2(t))$. To simplify the explanation, we adopt subscript k to designate the ordering of each tensor product B-spline basis function and its corresponding control point. Let s_{tr}^i be one of the surfaces resulting from tracing with parametric trimming curve c , $s_{\text{tr}}^i(\xi, \eta) = \sum_k N_k(\xi, \eta) r_{k,\text{tr}}^i$, where $r_{k,\text{tr}}^i \in \mathcal{R}_{\text{tr}}^i$, and its basis function is N_k . The least squares system is formulated as,

$$\text{minimize}_{\Delta r_k^i} \sum_u \left\| \sum_k N_k(c(t)) (r_{k,\text{tr}}^i + \Delta r_{k,\text{tr}}^i) - c_{e,\text{tr}}^i(t) \right\|^2,$$

where $\Delta r_{k,\text{tr}}^i$ is the unknown displacement vector of control points $r_{k,\text{tr}}^i$. Denote the set of updated control points as $\mathcal{R}_{\text{lstsq}}^i = \{r_{k,\text{lstsq}}^i = r_{k,\text{tr}}^i + \Delta r_{k,\text{tr}}^i\}$.

Next, the control points in $\mathcal{R}_{\text{lstsq}}^i$ are separated from each other across the trimming curves to avoid extra intersections in the surfaces. For that purpose, we create meshes of direction vectors in parametric space for $\mathcal{R}_{\text{lstsq}}^i$. Each mesh of parametric direction vectors is initialized to the 0 vector. Then the parametric trimming curve is sampled and for each sample, the curve normal direction pointing towards the interior of the trimmed parametric domain is computed. The basis function for each control point in $\mathcal{O}_{\text{lstsq}}^i$ is evaluated at the parametric samples. The normal direction of the sample(s) with the largest basis function value is assigned and denoted $v_{k,\text{sep}}^i$. The direction vectors associated with $\mathcal{O}_{\text{lstsq}}^i$ are then propagated to all direction vectors in each mesh by applying 50 iterations of Laplacian smoothing over the meshes of parametric direction vectors. Finally, we update the control mesh by moving the surface layer using these vectors assigned to each control point for a short distance to leave a gap around the trimming curve to create $\mathcal{R}_{\text{sep}}^i = \{r_{k,\text{sep}}^i = r_{k,\text{lstsq}}^i + \epsilon \hat{v}_{k,\text{sep}}^i\}$ where $\hat{v}_{k,\text{sep}}^i$ is $v_{k,\text{sep}}^i$ projected into model space using the fitted plane of $r_{k,\text{lstsq}}^i$'s local control mesh.

Then, a relaxation step is necessary because both the signed distance function and the harmonic field non-uniformly shrink distances between control points as they move inward. We apply Laplacian smoothing to the control mesh to get a target position \tilde{p} for each control point p and move p to $(1 - \beta)p + \beta\tilde{p}$ where β is a blending input parameter in $[0, 1]$, used to create \mathcal{R}^i .

Coefficients for the trim basis functions are obtained from curve fitting the midpoints of the sampled trim curves using the knot vectors from the parametric trimming curves. The set of coefficients is called Υ^i and is used with the appropriate trim basis functions. The trimmed surface layer \mathcal{G}^i (corresponding to control meshes \mathcal{R}^i) is transformed into \mathcal{B}^i , which is topologically identical to \mathcal{B} . Control points in \mathcal{R}^i are paired with corresponding revised basis functions; and control points in Υ^i are paired with appropriate trim basis functions. The resulting control lattice over all layers \mathcal{B}^i , along with the same degree d as the surface and uniform open knot vector (0 on \mathcal{B} and 1 on \mathcal{B}^n), defines a hybrid trivariate B-spline region \mathcal{I} .

4.3. Construction of Pyramid Elements

The interior boundary surface of \mathcal{I} must serve as a boundary for the unstructured remaining interior volume. The representation for the interior boundary surface of \mathcal{I} can use the dependent representations over each rectangular sub-knot interval to represent the base of a Bézier pyramid of degree d . The Bézier pyramid [4] has been shown to have the boundary geometry of Bézier triangles on each of the 4 faces, and a tensor product degree bi- d Bézier on its base surface. The collection of them then leaves only an unstructured volume \mathcal{U} bounded by degree d Bézier triangles that must be determined. Alternatively, if the interior boundary surface of \mathcal{I} were to directly interface with the unstructured region, there would need to be two tetrahedra over each rectangular sub-knot interval surface, each one of degree $2d$ as in [24, 20].

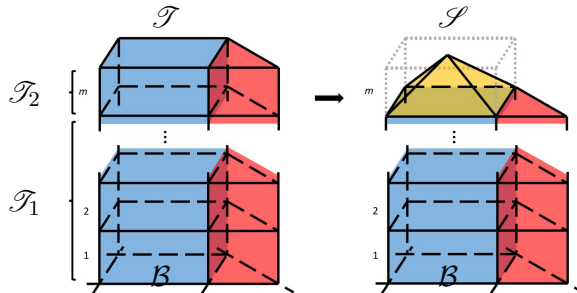


FIGURE 4.3. \mathcal{I} is converted to \mathcal{S} . Left: inward (upward direction) extensions of rectangular (blue) and triangular (red) sub-knot intervals. \mathcal{I} is divided into \mathcal{T}_1 and \mathcal{T}_2 . Right: The wedges in \mathcal{T}_2 are removed, and the tensor product Béziers in \mathcal{T}_2 are converted to pyramids (yellow). The semi-structured region \mathcal{S} is the union of three types of elements depicted in 3 colors. The inner boundary of \mathcal{S} consists only of Bézier triangles.

In creating the pyramid interface, care must be taken so that pyramids do not intersect each other. Since \mathcal{I} is constructed to have no self-intersections, it is subdivided in the inward direction into two trivariate splines, and the resulting innermost single knot interval trivariate is used to generate pyramids. \mathcal{T}_2 is the trivariate with a single knot interval in the inward direction that is transformed to the pyramid interface layer. The other multi-interior inward knot trivariate spline is called \mathcal{T}_1 .

The interior knot intervals and the sub-knot intervals from trimmed knot intervals and 3.4 are used to transform the representation in \mathcal{T}_2 to dependent trivariate Bézier representations. Each tensor-product Bézier volume from \mathcal{T}_2 is transformed to a Bézier pyramid whose coefficients are linear

combinations of those of its tensor-product Bézier volume (Figure 4.3). See [17] for details of the algorithm for the coefficients of pyramids. The control points with corresponding rational pyramid basis functions [4] define a pyramid element.

The semi-structured region consists of \mathcal{T}_1 and the pyramids, whose coefficients are linear combinations of coefficients from \mathcal{T}_2 . Thus, the only degrees of freedom are the ones from \mathcal{B}^i for $i \in \{0, 1, \dots, n\}$. The region is denoted \mathcal{S} . The degrees of freedom of \mathcal{S} is $(n + 1)(|\mathcal{R}| + |\mathcal{Y}|)$.

\mathcal{U} is an unstructured region with Bézier tetrahedral elements. Its boundary coincides with the inner surface of \mathcal{S} . It is constructed following [24]. The HV-rep is complete as $\mathcal{V} = (\mathcal{S}, \mathcal{U})$.

If instead, the user prefers to use unstructured Bézier hexahedra (trivariate patches), each element of \mathcal{U} can be transformed into an unstructured Bézier trivariate using reparameterization technique described in [21].

5. HB-Rep Error

Because Ω^{banded} is the only perturbed region that differs from the original B-spline surface, several attributes can be identified that affect the error in the HB-rep. Since this representation maintains parameterization, the error between \mathcal{G} and \mathcal{B} is measured by the Euclidean distance between the corresponding model space points evaluated at the same parametric value. The error has two attributes that matter in the effort to preserve the original representation: the area of Ω^{banded} and the error distance values. If a surface is flat, the curvilinear triangles in Ω^{banded} can represent the surface geometry exactly and distort the original parameterization minimally, but the HB-rep does not preserve the original B-spline representation. Consequently, it is preferred to keep Ω^{banded} narrow. On the other hand, a narrow Ω^{banded} also requires that the sub-knot intervals be small which results in shorter cubic trimming curve segments, and more trim functions.

Error in Ω^{banded} derives from two sources: the distance and curve parametrization error between Euclidean cubic trimming curve and the trimmed surfaces, and error of the approximated surfaces in curvilinear triangular sub-knot intervals. The former error comes from the input and is inherited from the imprecise nature of trimming curves themselves. In the HB-rep, it follows from the difference between the Euclidean trimming curve c_m and the parametric trimming curve composed with the surface mapping, given that it is required to exactly reproduce the Euclidean trimming curve to achieve watertightness. Since, for any given Bézier segment of a trimming curve, corresponding Bézier segments are all intended to represent the same curve, for any given value of t , $s_1(c_1(t))$, $s_2(c_2(t))$, and $c_m(t)$ represent the identical intersection point in model space. However, when s_i is a bicubic spline surface and c_i is piecewise cubic, $s_i(c_i)$ is a degree 18 curve, but c_m is only cubic, so there will be a shape distortion as well in a region of the surface near the trimming curve. The error in the trimming curve c_m provides a lower bound that can be achieved for the error in Ω^{banded} .

The other source of error is related to curvilinear triangular sub-knot intervals within Ω^{banded} . As discussed earlier, the surface mapping for curvilinear triangular sub-knot intervals in HB-rep is $\psi \circ \phi^{-1}$, which is different from the original B-spline surface mapping. To reduce the error, one choice would be to use the $\psi \circ \phi^{-1}$ combination but to optimize the location of the single interior control points for each of ψ and ϕ (for $d = 3$). Another is to use a degree $2d$ Bézier representation for ψ . Before matching c_m , the curvilinear geometry can be matched exactly to the image of the trimmed surface. Once c_m is matched, that mapping is still an approximation. Hence, one might optimize the interior control point locations based on both the surface and trimming curve. However, for $d = 3$, using $2d$ leads to 10 interior control points to optimize for each curvilinear triangle in the domain. The third alternative, the one we have adopted, is to reduce the error in Ω^{banded} by reducing its size, typically by subdividing Bézier segments where the error in the approximation is too large. Such a subdivision usually leads to two triangles, each about 1/4 the parent's size, and a rectangle that touches the

HYBRID REFINEMENT

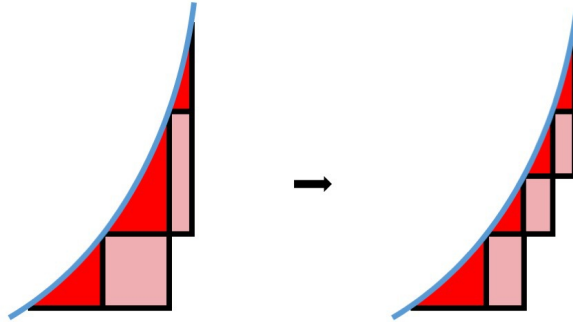


FIGURE 5.1. The trimming curve segment corresponding to the center curvilinear triangular sub-knot interval is subdivided into two pieces. The triangle is repartitioned into two curvilinear triangular and one rectangular sub-knot intervals. The two adjacent rectangular sub-knot intervals also change their shapes under the subdivision.

trimming curve at a corner. As the size of a curvilinear triangular sub-knot interval is reduced, ψ and its control mesh converge to the original B-spline surface because of the way the control points of ψ are defined. Furthermore, rectangular sub-knot intervals that were in Ω^{banded} typically become part of \mathcal{K} and represent the surface exactly so the error profile is reduced. Therefore, the HB-rep can converge to an exact trimmed representation under trimming curve refinement, subject to the error in c_m . This is illustrated in Figure 5.1 for subdivision of one curvilinear triangle.

		Quality of trimming curve approximation				
		0	1	2	3	4
trimming curve refinement level:	0	0.035	0.021	0.017	0.015	0.010
	1	0.029	0.018	0.010	0.0063	0.0035
	2	0.029	0.018	0.010	0.0063	0.0035

TABLE 5.1. Effects of trimming curve approximation and triangle refinement on surface max error

Shown in Table 5.1 is a demonstration of the effect of two ways to reduce surface max error for the model in Figure 4.2a. The columns correspond to different quality trimming curve approximations. Given discrete trimming data, the levels are simulated by creating cubic trimming curve approximations to the trimming curve data at multiple accuracy levels, with the 0 level being the least accurate. The rows correspond to subdividing that column's trimming curve at its previous row's midpoint to effectively create curvilinear triangles that are approximately one-fourth the previous rows size and approximating the surface over that triangle. For each column, a lower row always shrinks the area of the approximated surface. However, it does not reduce the maximum error of the approximated surface on the second trimming curve refinement level. That is because after first refinement the greatest error occurs on the trimming curve and, therefore, cannot be further reduced. Note that each level of subdivision reduces the area that is approximated in HB-rep

6. h -refinement

Refinement is used to add design degrees of freedom to a model and to discretize the model. By augmenting the original knot vectors with additional knot values, the original spline space is embedded

in a larger spline space with more degrees of freedom. The original model can be represented in terms of the basis of this larger space, but the added knots lower the derivative smoothness of the basis functions at those values. So changing coefficients in the new basis changes the model. In IGA, the term *h-refinement* refers to a similar concept that embeds a model in a larger spline space having new additional knots in each knot vector at the midpoints of every knot interval of the original knot vectors. Each knot interval, therefore, spawns 4 child knot intervals after refinement. Since IGA uses the same bases for simulation that are used to design the geometry models, refinement provides a way to maintain exact geometry while increasing the degrees of freedom for simulation under a process that makes elements uniformly smaller. Convergence estimates are frequently formulated in terms of multiple levels of *h-refinement*.

h-refinement is not straightforward for the HB-rep because of its complicated structure. Knot insertion in trimmed knot intervals can change the classification of resulting child sub-knot intervals. We investigate whether it would be preferable to apply *h-refinement* to an existing HB-rep \mathcal{B} , or to apply the *h-refinement* to the trimmed B-rep \mathcal{G} and then convert it to an HB-rep.

First, for a B-spline surface $s \in \mathcal{G}$, consider its untrimmed representation. Let μ and ν be the knot vectors, and let $\tilde{\mu}$ and $\tilde{\nu}$ be the refined knot vectors, with new knots added at the midpoints of each internal knot interval for each knot vector. Let $N_{i,j}$ be as before, and let $Q_{k,l}$ be B-spline basis functions resulting from the refinement. Then,

$$\begin{aligned} s(\xi, \eta) &= \mathbf{r}^\top \mathbf{N}(\xi, \eta) \\ &= \mathbf{r}^\top \mathbf{A} \mathbf{Q}(\xi, \eta), \end{aligned} \tag{6.1}$$

where \mathbf{r} is the vectorization of the coefficient matrix used to define the surface, $\mathbf{N}(\xi, \eta)$ and $\mathbf{Q}(\xi, \eta)$ are the corresponding vectors of original tensor product B-splines and refined tensor product B-splines, respectively, and $\mathbf{A} = \mathbf{A}_{\mu, \tilde{\mu}} \otimes \mathbf{A}_{\nu, \tilde{\nu}}$ the Kronecker tensor product of B-spline refinement operators in ξ and η directions. $\tilde{\mathbf{r}}^\top = \mathbf{r}^\top \mathbf{A}$ forms the refined control mesh with basis functions \mathbf{Q} .

Let $\mu \times \nu$ denote the knot intervals for the original B-spline representation and $\tilde{\mu} \times \tilde{\nu}$ denote the knot intervals after *h-refinement*. An interior knot interval $\mu \times \nu$ leads to 4 interior knot intervals in $\tilde{\mu} \times \tilde{\nu}$, as is usually the case. If $\mu \times \nu$ is exterior to the trimmed surface, its *h-refinement* children are also external, and none is used or referenced. For a trimmed knot interval, the case for which the trimming curves cross $\mu \times \nu$ is the more interesting one.

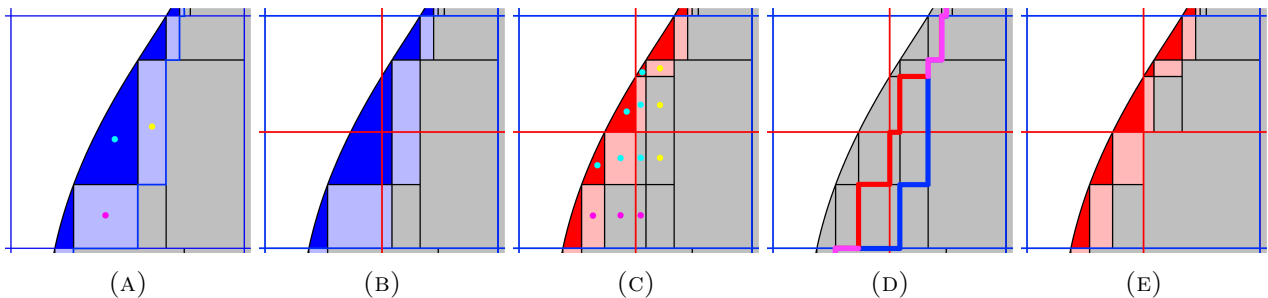


FIGURE 6.1. Partitions of a trimmed knot interval

With a partition \mathcal{K} already computed, the information can be reused to further divide sub-knot intervals in the partition that intersect new knot lines into smaller ones so that the resulting partition is valid. Figure 6.1 illustrates the effect of *h-refinement* on a single trimmed knot interval and Ω^{banded} . Note that Ω^{banded} must be recomputed locally since the trimming curve has been subdivided two times. In Figures 6.1a and 6.1b, it can be seen that some curvilinear triangular sub-knot intervals in Ω^{banded} at the top and the bottom of the figures remain unchanged because they do not cross any knot lines introduced by *h-refinement*.

HYBRID REFINEMENT

In Figure 6.1a the gray rectangular regions bounded by the black lines form \mathcal{K} . Ω^{banded} consists of the curvilinear triangles in dark blue, with an edge on the trimming curve, and the light blue rectangular regions touch the trimming curve at one point. In Figure 6.1b red lines show the knot interval refined into 4 child knot intervals. The knot lines cross the trimming curve in two places so there will need to be at least two more subdivisions of the trimming curve, with changes to the curvilinear triangular and rectangular sub-knot intervals. Figure 6.1c shows a refined classification. Note that the dark blue triangle with the cyan dot in Figure 6.1a has been partitioned into (i) three curvilinear triangle sub-knot intervals with cyan dots, (ii) two light red rectangles with cyan dots, each touching the trimming curve at a single point, and (iii) one gray rectangle that no longer belongs in Ω^{banded} . The light blue rectangle with the magenta dot has been subdivided into three rectangular knot intervals, only one of which should remain in Ω^{banded} . The light blue rectangular region with the yellow dot sustains partitioning in two from the refinement, with only the top rectangle properly surviving in Ω^{banded} . But requirements for it being adjacent to curvilinear triangles indicate its further subdivision. In Figure 6.1d boundaries of Ω^{banded} of the original and refined partitions are rendered with thick blue and red lines (with shared segments in magenta). Ω^{banded} gets narrower as h -refinement is applied to the surface.

Revised basis functions over the original dark blue triangle with the cyan dot functions are defined using appropriate $\psi \circ \phi^{-1}$, which includes cubic Bézier triangle functions composed with an inverse map, as are the trim basis functions. After refinement, a child of the curvilinear triangle can be a rectangular sub-knot interval that is no longer in Ω^{banded} (grey rectangle with a cyan dot in Figure 6.1c). This region in the unrefined watertight HB-rep cannot be reproduced by the refined HB-rep maintaining the same parameterization as well as geometry. This is because the unrefined representation has a surface mapping $\psi \circ \phi^{-1}$ which is not polynomial over the curvilinear triangle. But in the refined representation, it becomes a bivariate tensor product Bézier. A closer inspection of the introduced knot line going through the original curvilinear triangle in Figure 6.1b reveals that the straight line is mapped by ϕ^{-1} into a curved line in the canonical triangular domain. Therefore, the surface over an ostensibly simple rectangular domain cannot be expressed as a tensor product Bézier.

This approach also can lead to unnecessarily partitioned sub-regions of the trimmed knot interval. In Figure 6.1c, the lower right knot interval becomes an interior knot interval after h -refinement, and its partition within is unnecessary. However, because the partition after refinement is based on the partition of the original, the segmentations that existed for the unrefined case are kept, and refined, as necessary. Many rectangular sub-knot intervals in Ω^{banded} are not in the refined Ω^{banded} , or their child rectangles are not. Since they had one or more control points in the unrefined Υ that were modified to match the trimming curve, the children representations are also changed from the original surface. Such an example appears in the comparisons of Figure 6.1a and Figure 6.1c, where the light blue rectangle with the magenta dot is subdivided into one rectangle in refined Ω^{banded} and 2 rectangles that should be in \mathcal{K} . Thus, elements of \mathcal{K} can remain unchanged or be subdivided, depending on if refining knot lines cross them. But Ω^{banded} must be recomputed. Because a goal is to retain the original representation as much as possible, the child rectangular sub-knot intervals that become internal must have their representations reset to have coefficients obtained through Bézier extraction. The child rectangular sub-knot intervals and the child curvilinear triangles that are part of the refined Ω^{banded} are computed similarly, with control points partitioned into those that go with the refined revised basis functions and those that go with the refined trim basis functions. Because the trimmed knot interval was refined, the refined Ω^{banded} is of narrower extent, the size of the union of the children partitions continues to converge toward the trimming curve with each level of refinement. While the number and size of the sub-knot intervals in the union of the children refined \mathcal{K} are less optimal than if they were recomputed each time, they do not affect the refined revised basis functions, since, over those sub-knot intervals, the refined revised basis functions are identical to the refined B-splines. Their shapes are more relevant during integration and when they serve as the bases for the pyramid layer.

Consider instead the case for which the effect of h -refinement is considered initially only on the trimming curves. First, discuss a single trimmed surface. A later discussion presents the effect in a model. Each parametric trimming curve is refined wherever a new knot line crosses it. The Ω^{banded} constructed is the same one as results from constructing the Ω^{banded} for the unrefined trimmed knot intervals and then deriving the refined Ω^{banded} . Now there are four child knot intervals, some of whom may now be interior knot intervals, as in the lower right sub-knot interval of Figure 6.1e. The resulting union of the partitions of the child knot intervals has fewer elements than that obtained by refining the existing partition. Compare Figures 6.1c and 6.1e. The method differs from the one with partition already computed in that its \mathcal{K} usually has a better partition because the partitioning algorithm puts a priority on resulting partition quality over which integration has better characteristics and the pyramid base layer is better proportioned. Because the surface over the rectangular regions in \mathcal{K} is the same as the original B-spline surface, with its degrees of freedom totally dependent on those of the B-spline, the two methods differ neither in parameterization nor in geometry. However, while Ω^{banded} for the refined model is computed to be the same, this approach recomputes the representations for the surfaces over Ω^{banded} , as in the first case. So computing this type of h -refinement, while creating different sub-partitions \mathcal{K} , has exactly the same degrees of freedom as the first case's h -refinement.

The difference between the two approaches to h -refinement is apparent only when the HV-rep is considered. In both, the approximation in the Ω^{banded} region is recomputed attaining better accuracy while converging towards the trimming curves.

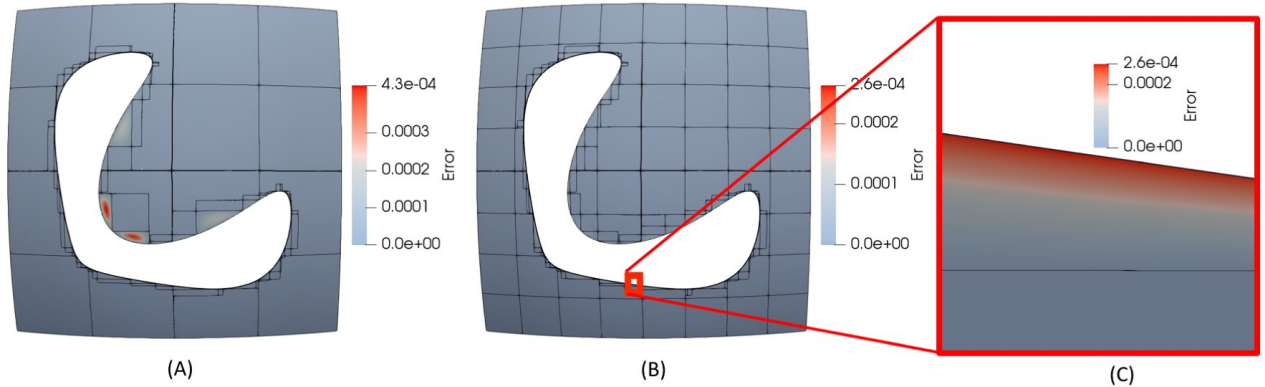


FIGURE 6.2. h -refinement is applied to a trimmed surface. (a) shows error on the original surface. The boundaries of sub-knot intervals in Ω^{banded} and surface knot lines are rendered in black. The result of h -refinement is shown in (b). An inset of the red rectangle is shown in (c). The max error after h -refinement occurs on the trimming curve.

An example of h -refinement on a trimmed surface is considered in Figure 6.2. A surface with 16 knot intervals is considered (6.2a). An L-shape hole is trimmed off from the surface creating 12 trimmed knot intervals and 4 interior ones. Initially, the greatest error occurs in the middle of curvilinear triangular sub-knot intervals. h -refinement is applied by uniformly inserting knots in each of the knot intervals in both directions. Partitions are recomputed, as is the HB-rep. The operation decreases both max error and the region where the error occurs (6.2b). Figure 6.2c shows an inset of the lower trimmed boundary of the L-shape. The greatest error occurs on the trimming curve. Therefore, it cannot be further reduced without a better trimming curve. Degrees of freedom in Figure 6.2a is $|\mathcal{R}| + |\Upsilon| = 49 + 204 = 253$. Degrees of freedom in Figure 6.2b is $121 + 237 = 358$.

The example above presents the effects when the single trimmed knot interval refinement is considered. Across the trimming curve in a trimmed B-rep, there might be different knot intervals that

reside in adjacent trimmed surfaces sharing one trimming curve corresponding to each curvilinear triangular sub-region this can lead to multiple recomputations of Ω^{banded} . A more efficient approach is to determine the effect of surface refinement on each surface across all trimming curves, and the new knots that should be added to each trimming curve. Then the new knots should be merged, so there is a refined trimming curve each of whose Bézier segments is a post h -refinement result. In this way, the refined Ω^{banded} may become significantly narrower with just a few levels of refinement.

6.1. h -refinement in \mathcal{S}

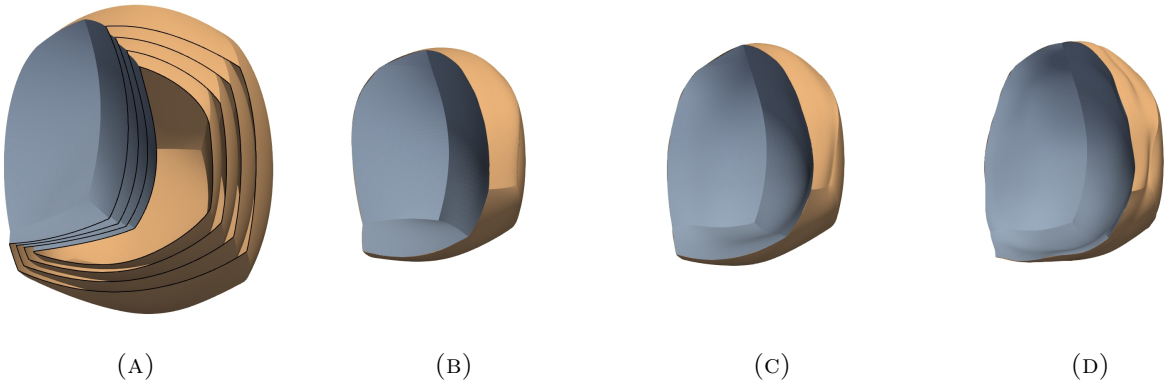


FIGURE 6.3. Given the HB-rep in Figure 4.2a, an HV-rep is generated with a trivariate representation to $\omega = 0.75$ (3/4 of the modified tracing distance toward the mid-structure). Several isolayers are shown in (a). \mathcal{T} is computed separately for each of 3 levels of h -refinement with the layers shown for $\omega = 0.75$ in (b) (the coarsest) through (d) (the finest).

When transforming an HB-rep into an HV-rep, other issues related to h -refinement can arise. Again we investigate several different approaches to refinement.

One approach is to perform h -refinement on the trimmed B-rep \mathcal{G} , then generate the corresponding HB-rep and HV-rep. If this is the chosen direction, then each control mesh is finer and moves closer to the surface than the control mesh that spawned it at the previous level. It is unclear if a different mid-structure would be appropriate for each of the refinements. Our experiment chose to use the same mid-structure, ensuring it was internal to all levels of refinements. In Figure 6.3, results from tracing and adjusting are shown by surface layers that have the same topology as \mathcal{B} . The model used in this example is the same one used in Figure 4.2a. It is constructed by subtracting one curved box from another. In Figure 6.3a, a planar cutaway shows several internal layers of both gold and gray surfaces. The innermost layer shown corresponds to $\omega = 0.75$ is shown in Figure 6.3b. Figure 6.3c and 6.3d show the same layer computed separately for each of 2 levels of h -refinement. Each control lattice was computed from an HB-rep that started from unrefined (Figure 6.3b), one level of h -refinement (Figure 6.3c), and two levels of h -refinement (Figure 6.3d). There is an artifact visible towards the right side of Figure 6.3d that does not exist in Figure 6.3b and is only slightly visible in Figure 6.3c. The most refined inner surfaces seem to have a wrinkle near \mathcal{O} . We deduce that it is caused in the adjustment phase. During the adjustment phase, in order to modify intersecting trimmed surface (Figure 4.2b), control points around trimming curves are moved towards the interior direction of the respective surface. Since the control mesh is denser after refinement, when the same moving parameter (ϵ as used in [17]) is used, as in this experiment, control points in \mathcal{O} are more likely to overshoot a

reasonable location, thus forming a wrinkle. Adjusting ϵ to be related to refinement level can alleviate the problem.

This type of artifact is observed only near trimming curves with acute dihedral angles, usually formed by Boolean subtraction or intersection. A union, on the contrary, does not cause this artifact. For example, in Figure 4.2d, the inner layer of a tetrapod is shown. The tetrapod is a union of four capsule shapes. The adjustment phase is not included in this example to demonstrate more clearly the gaps between trimmed surfaces as the tracing paths increase in depth. Because the adjustment phase moves control points towards the trimming curves and brings them closer, wrinkles are not formed.

Alternatively, refinement can occur after the control lattices of the trivariates are computed. After tracing and adjustment are applied, a control lattice of the coarse control mesh without h -refinement is generated. Corresponding control points \mathcal{R}^i and trimmed surface layers \mathcal{G}^i are computed, to generate h -refinement of the control lattice. After h -refinement, at each layer, appropriate knots due to h -refinement are inserted into the trimming curves, they are made compatible and Ω^{banded} is formed for each surface in \mathcal{B} , and percolated into each layer. The resulting interior isolayers are modified only slightly by the trimming surface with that recomputation, while, as previously discussed, the boundary layer, the refined \mathcal{B} more accurately approximates the original surfaces near the trimming curves.

So far, there has been no discussion of the effects of trivariate refinement on the inner boundary surface (of \mathcal{T}_1) that serves as the base layer for the pyramid interface and the unstructured region. In general, the knot interval behavior of innermost surface in \mathcal{T}_1 is the same as that for \mathcal{B} , and corresponds to interior knot intervals, interior sub-knot intervals in the \mathcal{K} , and sub-knot interval behavior in Ω^{banded} . The B-spline representation is used over the knot intervals and partitions of the \mathcal{K} , so a particular partitioning into elements does not affect the refined representation. However, the pyramids are defined in using the innermost surface partitioned according to the knot intervals and sub-knot intervals in the partition \mathcal{K} as their bases. Therefore, the partition affects the pyramids, as its refinements cause the pyramid and unstructured region to also be refined or modified. After h -refinement, all interior knot intervals used to create the pyramids of the unrefined HV-rep can be directly refined in a standard manner. Those elements form the bases of refined pyramids, using the approach in [7]. So refined interior intervals and refined pyramids over them follow directly. Adjacent tetrahedra can be refined in a compatible manner [7].

The refined pyramid region above refined trimmed knot intervals, including \mathcal{K} , is more complex to define. For a simpler presentation, assume that given a parent trimmed interval, there is the parent Ω^{banded} and the refined Ω^{banded} that is the union of the Ω^{banded} for all the child trimmed sub-knot intervals. Further, Let K be the residual rectilinear region in the trimmed knot interval after Ω^{banded} is extracted. Then \mathcal{K} is a partitioning of K . Suppose there are four child knot intervals, each either an interior knot interval or a trimmed knot interval of the refined HB-rep surface. The child trimmed knot intervals each have their own child partition, \mathcal{K}^c . Intersections of elements in \mathcal{K}^c with those in \mathcal{K} can lead to a need to subdivide existing pyramids above elements in \mathcal{K} in irregular, complicated, ways that do not preserve the idea of *uniform* refinement in h -refinement, and lead to poorly shaped Bézier pyramids. Instead, the trivariate spline layer \mathcal{T}_2 is used to define new child pyramids with heights related to the dimensions of their bases. An interior child knot interval and its new pyramid have a standard representation for further refinements. For a child trimmed knot interval, the pyramid is again recomputed adapted to the size of base. This is also done for the rectangular elements in Ω^{banded} . These elements over the child Ω^{banded} and the child \mathcal{K} need to be recomputed with each subsequent refinement until they can be removed as interior child knot intervals. Then they would be standard elements. In addition to recomputing the pyramids, tetrahedra that are neighbors (face, edge, vertex) of the parent pyramids adjacent to the pyramids that need recomputation must be removed. Then the empty region bounded by refined pyramids, recomputed pyramids, and refined tetrahedra must be re-tetrahedralized.

Convergence properties of B-splines with each level of refinement guarantee that child trimmed knot intervals may increase in number, but they will decrease in area, and converge towards the trimming surface in the trivariate lattice. Thus the regions requiring re-pyramidalization and re-tetrahedralization get progressively smaller.

7. Conclusion

Volumetric model completion from trimmed B-reps is a nascent focus of recent research. Simulations frequently require volumetric representations that are not native to CAD systems. Trimmed B-reps are integral to design yet their inexactness causes significant problems for analysis. The discussed HB-rep and HV-rep can be recomputed if the trimmed B-rep changes, when, for example, surfaces are modified relative to each other.

Hybrid representations have the drawbacks of requiring multiple refinement and subdivision schemes that are compatible. While h -refinement has one standard meaning for B-splines and NURBS curves, surfaces, and volumes, there are multiple refinement schemes for triangles and tetrahedra, any one of which can be used in a simulation.

Revised basis functions and trim basis functions cannot be exactly refined, since they are not polynomial near the trimming curves. The partitions near the trimming curve that are used in defining them are not refined uniformly when h -refinement is performed on the trimmed B-spline B-rep model. This causes significant complexity in formulating appropriate definitions for h -refinement.

We discuss strategies to apply h -refinement on HB-rep along with corresponding consequences. In general, the HB-rep cannot maintain its parameterization and geometry during h -refinement within Ω^{banded} . However, as an HB-rep is refined, the region preserving the original parameterization and geometry increases. The error introduced by triangular curvilinear sub-knot interval approximation is reduced. As that error reduces, error inherited from the trimming curve eventually dominates, and cannot be further reduced without a better-fitted trimming curve. The user has the option to keep the partition information from the unrefined partition for \mathcal{K} in each trimmed knot interval. By keeping the partition from the unrefined \mathcal{K} , the region that requires computation of new pyramids and tetrahedra is reduced with each refinement. However, if the shape and size of the pyramids become an issue, computing new partitions over each refined trimmed knot interval can lead to better pyramids, also of reduced size. Then tetrahedralization is required only over the region bounded by the refined tetrahedra and pyramids over internal knot intervals from the previous level. These regions requiring recomputation are also reduced since refinement of trimmed knot intervals eventually leads to interior child intervals, except adjacent to trimming curves.

The hybrid representation with no trimming curves can be refined using B-spline h -refinement in the tensor product trivariate region, with compatible refinements as proposed in [7] for pyramids and Bézier tetrahedra. We have demonstrated that a straightforward approach cannot be directly applied to the HB-rep and the HV-rep. Although one approach might be to create new HB-reps and HV-reps for each refinement, we have demonstrated that the HB-rep on the refined representation is the same as refining the HB-rep of the unrefined representation. However, we have also demonstrated that unless parameters are carefully adjusted, HV-reps computed after several levels of refinement can have a reduced quality in the interior, compared to applying modified refinement to the original HV-rep.

We have presented two new approaches to refinement that support an h -refinement convergent approach (in a B-spline manner) that simultaneously refine the representation and ensure that the representation converges to the original surfaces, while still maintaining a consistent HV-rep.

References

- [1] H. Al Akhras, T. Elguedj, A. Gravouil, and M. Rochette. Isogeometric analysis-suitable trivariate NURBS models from standard B-Rep models. *Computer Methods in Applied Mechanics and Engineering*, 307:256–274, 2016.
- [2] H. Al Akhras, T. Elguedj, A. Gravouil, and M. Rochette. Towards an automatic isogeometric analysis suitable trivariate models generation-Application to geometric parametric analysis. *Computer Methods in Applied Mechanics and Engineering*, 316:623–645, 2017.
- [3] M. J. Borden, M. A. Scott, J. A. Evans, and T. J. R. Hughes. Isogeometric finite element data structures based on Bézier extraction of NURBS. *International Journal for Numerical Methods in Engineering*, 87(1-5):15–47, 2011.
- [4] J. Chan and T. Warburton. A Short Note on a Bernstein–Bézier Basis for the Pyramid. *SIAM J. Sci. Comput.*, 38(4):A2162–A2172, 2016.
- [5] E. Cohen, R. F. Riesenfeld, and G. Elber. *Geometric modeling with splines : an introduction*. A. K. Peters, 2001.
- [6] J. A. Cottrell, T. J. R. Hughes, and Y. Bazilevs. *Isogeometric Analysis: Toward Integration of CAD and FEA*. Wiley Publishing, 1st edition, 2009.
- [7] L. Engvall and J. A. Evans. Isogeometric unstructured tetrahedral and mixed-element Bernstein–Bézier discretizations. *Computer Methods in Applied Mechanics and Engineering*, 319:83–123, 2017.
- [8] X. Gao, T. Martin, S. Deng, E. Cohen, Z. Deng, and G. Chen. Structured Volume Decomposition via Generalized Sweeping. *Visualization and Computer Graphics, IEEE Transactions on*, PP(99):1–1, 2015.
- [9] L. Liu, Y. Zhang, T. J. R. Hughes, M. A. Scott, and T. W. Sederberg. Volumetric T-spline construction using Boolean operations. *Engineering with Computers*, 30(4):425–439, 2014.
- [10] T. Martin and E. Cohen. Volumetric parameterization of complex objects by respecting multiple materials. *Computers & Graphics*, 34(3):187–197, 2010. Shape Modelling International (SMI) Conference 2010.
- [11] T. Martin, E. Cohen, and R. M. Kirby. Mixed-element volume completion from NURBS surfaces. *Computers & Graphics*, 36(5):548–554, 2012. Shape Modeling International (SMI) Conference 2012.
- [12] B. Marussig and T. J. R. Hughes. A Review of Trimming in Isogeometric Analysis: Challenges, Data Exchange and Simulation Aspects. *Archives of Computational Methods in Engineering*, 25(4):1059–1127, 2018.
- [13] J. O’Rourke and G. Tewari. The structure of optimal partitions of orthogonal polygons into fat rectangles. *Computational Geometry*, 28(1):49–71, 2004. 14th Canadian Conference on Computational Geometry-CCCG02.
- [14] T. W. Sederberg, G. T. Finnigan, X. Li, H. Lin, and H. Ipson. Watertight Trimmed NURBS. In *ACM SIGGRAPH 2008 Papers*, pages 79:1–79:8. ACM, 2008.
- [15] J. Shen, J. Kosinka, M. A. Sabin, and N. A. Dodgson. Conversion of trimmed NURBS surfaces to Catmull-Clark subdivision surfaces. *Computer Aided Geometric Design*, 31:486–498, 2014. Recent Trends in Theoretical and Applied Geometry.
- [16] J. Shen, J. Kosinka, M. A. Sabin, and N. A. Dodgson. Converting a CAD model into a non-uniform subdivision surface. *Computer Aided Geometric Design*, 48:17–35, 2016.
- [17] Y. Song and E. Cohen. Creating Hybrid B-Reps and Hybrid Volume Completions from Trimmed B-Spline B-Reps. Technical report, School of Computing, University of Utah, 2019.
- [18] Y. Song and E. Cohen. Making Trimmed B-Spline B-Reps Watertight With a Hybrid Representation. In *International Design Engineering Technical Conferences and Computers and Information in Engineering Conference*, 2019. to appear.

HYBRID REFINEMENT

- [19] S. Xia and X. Qian. Isogeometric analysis with Bézier tetrahedra. *Computer Methods in Applied Mechanics and Engineering*, 316:782–816, 2017. Special Issue on Isogeometric Analysis: Progress and Challenges.
- [20] S. Xia, X. Wang, and X. Qian. Continuity and convergence in rational triangular Bézier spline based isogeometric analysis. *Computer Methods in Applied Mechanics and Engineering*, 297:292–324, 2015.
- [21] G. Xu, Y. Jin, Z. Xiao, Q. Wu, B. Mourrain, and T. Rabczuk. Exact conversion from Bézier tetrahedra to Bézier hexahedra. *Computer Aided Geometric Design*, 62:154–165, 2018.
- [22] G. Xu, B. Mourrain, R. Duvigneau, and A. Galligo. Analysis-suitable volume parameterization of multi-block computational domain in isogeometric applications. *Computer-Aided Design*, pages 395–404, 2013.
- [23] G. Xu, B. Mourrain, R. Duvigneau, and A. Galligo. Constructing analysis-suitable parameterization of computational domain from CAD boundary by variational harmonic method. *J. Comput. Phys.*, 252:275–289, 2013.
- [24] S. Zeng and E. Cohen. Hybrid Volume Completion with Higher-order BéZier Elements. *Comput. Aided Geom. Des.*, 35(C):180–191, 2015.
- [25] Y. Zhang, W. Wang, and T. J. R. Hughes. Solid T-spline construction from boundary representations for genus-zero geometry. *Computer Methods in Applied Mechanics and Engineering*, 249-252:185–197, 2012. Higher Order Finite Element and Isogeometric Methods.